



Contents lists available at ScienceDirect

Microporous and Mesoporous Materials

journal homepage: www.elsevier.com/locate/micromeso

Vanadosilicate with MWW zeolite structure synthesized from VCl_3 by cooperative assembly of organic templates

Thiago F. Chaves^{a,c,*}, Aline R. Passos^b, Valérie Briois^b, Leandro Martins^a, Sandra H. Pulcinelli^a, Celso V. Santilli^a, Joaquín Pérez-Pariente^c

^a Instituto de Química, Unesp – Univ. Estadual Paulista, Rua Prof. Francisco Degni 55, 14800-060, Araraquara, SP, Brazil

^b Synchrotron SOLEIL, L'Orme des Merisiers, Saint-Aubin, BP 48, Gif-sur-Yvette, F-91192, France

^c Instituto de Catálisis y Petroleoquímica, ICP-CSIC, C/Marie Curie 2, 28049, Madrid, Spain

ARTICLE INFO

Keywords:

MWW
Vanadosilicate
Mixed templates
 V^{3+} and V^{4+}

ABSTRACT

Aluminum-free MWW structure containing vanadium was easily prepared from a mixture of suitable templates (*N,N,N*-trimethyl-1-adamantonium hydroxide (TMAdaOH) and hexamethyleneimine (HMI)). Besides, the use of VCl_3 as vanadium source, in which this metal is in low oxidation state (V^{3+}) and the preparation of the synthesis gel under inert atmosphere are crucial to get an efficient incorporation of vanadium into the zeolitic framework. UV–Vis spectrum of the as-synthesized material whose oxidation was prevented by working under inert atmosphere reveals the presence of isolated V^{3+} sites isomorphically coordinated. Besides, the ^{29}Si MAS NMR spectra and the V K-edge X-ray Absorption Spectroscopy (XAS) analysis show that the vanadium was incorporated into the zeolite framework with formation of V–O–Si linkages. ^{13}C MAS NMR evidences that both templates are present in the as-synthesized material, showing that the mixture of TMAdaOH and HMI is crucial for obtaining pure crystalline vanadosilicate phase. XAS measurements of the V-containing zeolite during calcination under air showed that initially the sample contains V^{4+} sites in a square pyramidal geometry, which were completely oxidized to isolated V^{5+} in T_d coordination after calcination.

1. Introduction

According to the classical definition, zeolites are hydrated aluminosilicates of open crystalline structure composed of tetrahedrally coordinated Si and Al atoms linked together by oxygen atoms. However, due to the breakthrough of similar structures containing other tetrahedrally coordinated (P, Fe, Ge, Ga, B, Sn, V, etc.) elements, the term “zeotype” has been coined to describe these new structures [1,2]. A landmark in the attempts for heteroatom insertion in microporous molecular sieves was the discovery of a titanosilicate with MFI structure (TS-1) [3] and its successful application as redox catalyst. Afterwards, large efforts have been done to incorporate other metals (for example Fe, Cr, Co and V) into the microporous framework and to study their application as catalysts in liquid phase oxidations [4]. Isomorphous substitution of framework tetrahedrally coordinated Si and Al atoms for a variety of metal ions with sizes suitable to fit into the tetrahedral sites of these structures is an important field of synthetic zeolite chemistry [5].

Vanadium substitution has been achieved in several microporous and mesoporous molecular sieves to yield materials such as V-MFI, V-

MEL, V-BEA, V-MRE, [V,Al]-MCM-22, EVS-10, V-MCM-41, and V-MCM-48 [6–13]. Endeavors have been made to incorporate vanadium into the zeolite framework in order to develop the Lewis acidity in the catalytic systems [14,15] and also for oxidation of various substrates [16–19]. Zeotypes containing vanadium can be obtained by the partial substitution of the Si^{4+} and/or Al^{3+} T sites and also as Al-free structures. Incorporation of vanadium can be performed by two main methods, post-synthesis modification and direct hydrothermal synthesis. In the latter case, the synthesis parameters should be optimized for each type of structure [4]. Al-free vanadosilicates are difficult to crystallize because, in general, the presence of Al species is important during the nucleation and growth of zeolites. The first pure, Al-free vanadium containing zeolites were MFI and MEL [6,7], probably because they can also be obtained in all-silica form.

The isomorphous substitution is an efficient method to incorporate heteroatom into the framework, replacing the tetrahedral silicon. The catalytic properties of microporous and crystalline titanium-silicates, for example the TS-1 (MFI framework), are rigorously associated with the structural particularities of the silica framework [20,21]. In contrast to bulk systems, such as mixed oxides or supported V_2O_5 , the exchange

* Corresponding author. Instituto de Química, Unesp – Univ. Estadual Paulista, Rua Prof. Francisco Degni 55, 14800-060, Araraquara, SP, Brazil.

E-mail address: faheina@yahoo.com.br (T.F. Chaves).

<https://doi.org/10.1016/j.micromeso.2018.12.030>

Received 13 August 2018; Received in revised form 20 November 2018; Accepted 19 December 2018

Available online 21 December 2018

1387-1811/ © 2019 Elsevier Inc. All rights reserved.

of oxygen between the catalyst and the reagent is limited by diffusion of oxygen vacancies through the oxide lattice [22,23]. Based on this limitation, isolated catalytic sites in vanadosilicates structure can auxiliary the exchange of oxygen and Mars-van Krevelen redox dynamic mechanism V^{5+} and V^{4+} .

Layered materials may be used as precursors for the synthesis of many other zeolite structures, for example, magadiite, kanemite, MCM-22(P), PREFER, ITQ-2 and ITQ-6 [24–27]. Alongside, these layered materials may be modified by various methods such as ion-exchange, condensation between the lamellae, pillarization, and silylation, among others. The possibility of modification of the lamellar zeolitic materials for a wanted application makes them particularly suitable for catalysis [28]. MWW is among the most interesting zeolite family, because it contains two independent pore systems and during the synthesis a lamellar precursor is obtained, providing very interesting properties to this material [29]. It is well known that MWW zeolite contains a two channel system consisting of 10-membered-ring (MR) viewed to crystallographic direction [001] between “layers” (0.48×0.35 nm and 0.41×0.51 nm). One pore system is composed of 12 MR MWW cages with dimensions of $1.82 \times 0.71 \times 0.71$ nm. The MWW cages are connected to one another through 10 MR windows. The second is a two-dimensional (2D) 10 MR pore system that does not contain any cages [30]. For MWW structure, and to the best of our knowledge, the synthesis of pure Al-free vanadosilicate with MWW structure has not been reported so far, and only the partial substitution of Al sites via direct synthesis has been published ([V,Al]-MWW) [10].

Concerning the isomorphous substitution of metals in zeolite materials by direct synthesis methodologies, little attention has been paid to the oxidation state of the metal. On this regard, it has been reported recently that $TiCl_3$ can be used to crystallize the large-pore Ti-containing aluminophosphate with AFI structure TAPO-5, which shows improved catalytic properties in the mild oxidation of cyclohexene as compared with the TAPO-5 materials synthesized from conventional Ti (IV) sources [31–34]. On these bases, we have investigated the effect of OSDA (Organic Structure Directing Agent) to synthesize Al-free MWW vanadosilicate by using a vanadium source in low oxidation state, namely VCl_3 . The purpose of using V^{3+} is to facilitate the isomorphous substitution of this metal in the zeolite framework, because it could eventually behave as Al^{3+} from the point of view of charge balance, avoiding at the same time the formation of unwanted V–O–V chemical species. It will be evidenced from this detailed study that this is an efficient route to obtain MWW vanadosilicates in the absence of aluminum. Herein the different V-species present in as-synthesized and calcined samples have been identified, and the influence of the protocol

of preparation on the effective incorporation of vanadium in the lattice of the MWW structure has been discussed.

2. Materials and methods

2.1. Synthesis of the MWW vanadosilicates

The synthesis of V-MCM-22 zeolite was attempted according to the procedures described by Pérez-Pariente et al. [35] for pure aluminosilicate using hexamethylenimine (HMI) as the structure directing agent. Briefly, the required amounts of sodium hydroxide (NaOH, Sigma-Aldrich) and hexamethylenimine (HMI, Sigma-Aldrich) were added to water. Thereafter, the source of vanadium (VCl_3 or $VOSO_4$, Sigma-Aldrich) was added and kept under stirring for 30 min. Then, the silica source Aerosil® (SiO_2 , Evonik) was added gradually and remained under stirring for another 30 min. The resulting gels were then introduced into teflon-lined stainless steel autoclaves and heated at $150^\circ C$ for 7 days under stirring at 60 rpm. After that, the autoclaves were cooled in cold water, the samples were recovered by filtration, washed, and dried in air at ambient temperature overnight. The samples with MCM-22 code were prepared following this composition: 1 SiO_2 : 0.017 V_2O_3 : 0.09 Na_2O : 0.5 HMI: 44.9 H_2O . The synthesis using VCl_3 was performed under N_2 atmosphere inside of a glove bag to prevent oxidation of the vanadium precursor.

The samples with ITQ-1 code were synthesized according to a procedure described previously by Cambor et al. [36] for the synthesis of ITQ-1 (all-silica MWW structure). All syntheses were carried out hydrothermally under stirring at $150^\circ C$ in basic medium and in the absence of alkali cations. The vanadosilicates were prepared at ambient temperature under N_2 atmosphere inside of a glove bag by employing Aerosil® (SiO_2 , Evonik), vanadium chloride (VCl_3 , Sigma-Aldrich), hexamethylenimine (HMI, Sigma-Aldrich) and *N,N,N*-trimethyl-1-adamantanium hydroxide solution (TMAdaOH 25% wt., SACHEM) as OSDA. TMAdaOH and HMI were mixed in water and then vanadium chloride (or $VOSO_4$) was added. The solution remained under stirring for 1 h. After this, Aerosil® was added slowly so that the resulting synthesis mixture reached a molar composition of 1 SiO_2 : x V_2O_3 : 0.31 HMI: 0.25 TMAdaOH: 44 H_2O , where, x = 0.025, 0.017, 0.013 or 0.008. Different synthesis gels (Si/V ratio) were obtained by varying the amount of vanadium as indicated by the values of x. The mixture was transferred to Teflon-lined autoclaves, sealed and heated at $150^\circ C$ under autogenous pressure for 7 or 14 days under stirring at 60 rpm. After cooling to room temperature (RT), the resulting solid was recovered by filtration on a Büchner funnel, washed with deionized

Table 1
Chemical composition, crystallinity and synthesis conditions of all samples obtained in this study.

Sample ^{a,b}	Si/V gel	Si/V EDS	V Source	C/N	CHN (%)	TG (%)	Time (days)	Phase
1V-MCM-22	30	NA ^c	VCl_3	NA	NA	NA	7	Amorphous
2V-MCM-22	30	NA	$VOSO_4$	NA	NA	NA	7	Amorphous
ITQ-1	∞	NA	–	10.2	19.2	22.0	7	MWW
1V-ITQ-1	20	35.4	VCl_3	NA	NA	12.2	7	MWW
2V-ITQ-1	20	27.6	VCl_3	NA	NA	11.3	14	MWW
3V-ITQ-1	30	26.5	VCl_3	10.1	11.3	14.2	7	MWW
4V-ITQ-1	30	29.1	VCl_3	NA	NA	13.7	14	MWW
5V-ITQ-1	40	NA	VCl_3	NA	NA	NA	7	MWW
6V-ITQ-1	40	NA	VCl_3	NA	NA	NA	14	MWW
7V-ITQ-1	60	53.5	VCl_3	10.2	16.8	20.0	7	MWW
8V-ITQ-1	60	51.2	VCl_3	NA	NA	17.7	14	MWW
9V-ITQ-1	30	87.9	$VOSO_4$	NA	NA	NA	7	MWW
10V-ITQ-1 ^c	30	204.4	VCl_3	NA	NA	NA	7	MWW
11V-ITQ-1 ^d	30	NA	VCl_3	NA	NA	NA	7	Amorphous

^a Samples with MCM-22 code were prepared following this composition: 1 SiO_2 : x V_2O_3 : 0.09 Na_2O : 0.5 HMI: 44.9 H_2O .

^b Samples with ITQ-1 code were prepared following the composition: 1 SiO_2 : x V_2O_3 : 0.25 TMAdaOH: 0.31 HMI: 44 H_2O .

^c The samples synthesized using VCl_3 were prepared under air atmosphere.

^d Sample synthesized without HMI.

^e NA stands for “Not analyzed”.

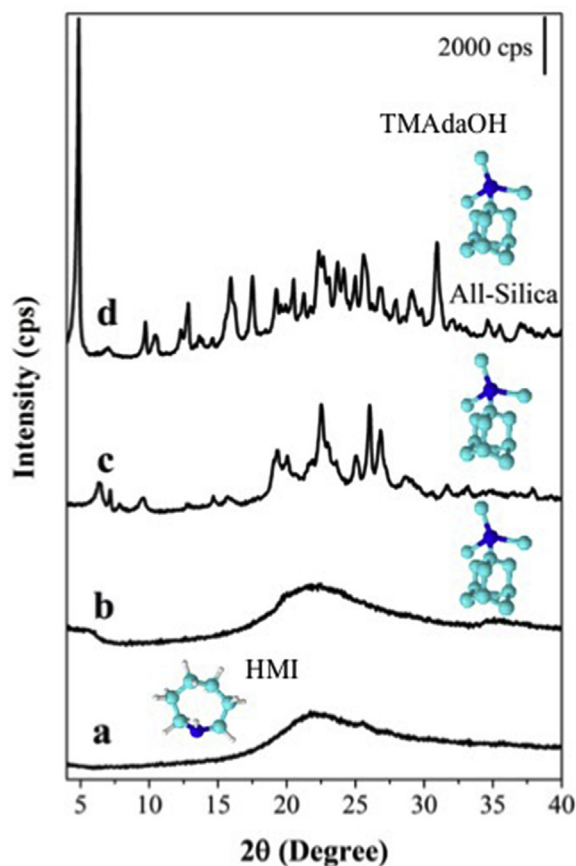


Fig. 1. XRD results for samples synthesized by different synthesis protocols using HMI and/or TMAdaOH as SDA: (a) MCM-22 method, (b), (c) and (d) ITQ-1 method. Synthesis conditions: (a), (b) and (c) Si/V = 30, (d) all-silica; 150 °C for 7 days under stirring.

water, and dried in air at RT. When necessary for specific characterizations, the sample was dried under N₂ atmosphere in the glove bag. Table 1 collects the specific synthesis conditions of the several materials together with some of their chemical and physical properties.

2.2. Characterization

X-ray diffraction (XRD) patterns were recorded on a X'Pert Pro PANalytical diffractometer with Cu K α radiation at a scan rate of 2°/min and a step size of 0.02°. Relative crystallinity has been estimated for the synthesized samples considering the area of the (310) diffraction peak. Diffuse reflectance UV–Vis spectra (DR–UV–Vis) were recorded in the UV–Vis–NIR region on a Varian Cary 5000 spectrometer. Thermogravimetric analysis was conducted using a Perkin-Elmer TGA7; the sample was heated at 20 °C/min under synthetic air flow (100 mL/min). ATR-IR spectroscopy measurements were performed using the Platinum Diamond Micro-ATR accessory accoupled to Bruker VERTEX 70 FTIR spectrometer.

Scanning electron microscopy was performed using a Hitachi S–3000N equipment. The samples were previously deposited on a carbon tape placed on a sample-holder and sputtered with gold. Energy Dispersive Spectroscopy measurements were acquired in the same microscope and the quantitative speciation results were done by average of at least five analyses in different regions of the sample. High resolution transmission electron microscopy (HRTEM) images were taken on a FEI Tecnai G² 20 transmission electron microscopy with an acceleration voltage of 200 kV.

N₂ physisorption isotherms were measured at 77 K using an ASAP 2010 Micromeritics instrument. The samples were outgassed for 24 h at

200 °C prior to measurement. The external specific area and micropore volume were calculated using the t-plot method and the mesopore size distribution was determined by the Barret-Joyner-Hallenda (BJH) method [37].

The solid state ²⁹Si MAS NMR and ¹H–¹³C CP MAS spectra were recorded using a Bruker MSL 400 spectrometer. ²⁹Si MAS NMR was performed working at 59.6 MHz, with a pulse delay of 0.5 s and a rotor spinning rate of 4.5 kHz. Additionally, ²⁹Si CP/MAS NMR spectra were acquired with 2 ms of the contact time, and proton decoupling. Chemical shifts were referenced to tetramethylsilane (TMS), used as external standard.

X-ray Absorption Spectroscopy (XAS) measurements were performed at the vanadium K-edge (5465 eV) at the ROCK beamline [38] of the SOLEIL synchrotron facility. The ITQ-1 vanadosilicate sample with ratio Si/V = 30 was prepared as pellet diluted in BN and measured at liquid nitrogen temperature (77 K). Time-resolved Quick-XAS measurements on the same sample were performed during *in situ* calcination using a dedicated cell [39] with flow of 20 mL/min O₂/He and heated from RT to 550 °C at a rate of 10 °C/min followed by 1 h of isothermal treatment. Normalization of the XAS data was performed by using the Python normal_gui graphical interface developed at SOLEIL for the fast handling of the Quick-XAS data. The data were energy-calibrated using a metallic vanadium foil recorded simultaneously with the sample and setting the first derivative maximum at 5465 eV.

The vanadium speciation during calcination was determined by multivariate data analysis, using the so-called Multivariate Curve Regression with Alternating Least Square (MCR-ALS) method. Details about the use of MCR-ALS method applied to XAS can be found in previously published works [40,41]. EXAFS spectra were extracted from the raw absorption signal using the Athena software graphical interface [42]. Structural parameters were obtained through the least-square fitting of the Fourier-transformed k³ $\chi(k)$ EXAFS data using the Artemis software graphical interface [42]. To fit the EXAFS data, values of E₀ used for k-scaling and S₀² the amplitude reduction factor were both obtained by fitting the EXAFS of a crystalline V₂O₄ reference with the number of nearest neighbor atoms (N) and their distances (R) fixed at their expected crystallographic values [43]. The values obtained (E₀) 5479.1 eV and (S₀²) 1.16 were then used for modeling the EXAFS signals of the ITQ-1 (Si/V = 30) sample measured at 77 K and of its calcined product measured at RT after calcination at 500 °C under air. The number of fitted points satisfies the number of independent points available in the data set, according to the Nyquist criterion [44]. The fit quality was determined using the EXAFS reliability factor R_F, which measures the relative misfit with respect to the data.

3. Results

3.1. Effect of organic structure directing agent (OSDA)

In this study, the MCM-22 synthesis protocol reported by Pérez-Pariante et al. [35] in the presence of aluminum, but avoiding herein in this case the addition of this element to the synthesis gels, and the ITQ-1 protocol by Cambor et al. [36] for all-silica materials were both investigated. In the MCM-22 route, only HMI was employed as SDA and in the ITQ-1 route a mixture of templates was used (HMI and TMAdaOH). The XRD results are presented in Fig. 1. The syntheses performed from the MCM-22 protocol [35] using only HMI (Fig. 1a) or only TMAdaOH (Fig. 1b), resulted in the formation of an amorphous solid. Using the ITQ-1 protocol (Fig. 1c, HMI and TMAdaOH) a product with the typical MWW diffraction pattern was obtained.

To evaluate the influence of HMI as an auxiliary OSDA in the ITQ-1 protocol, additional syntheses were performed employing only TMAdaOH without vanadium source. Fig. 1d shows the characteristic XRD pattern of the resulting sample. When the synthesis was performed in all-silica system in presence of TMAdaOH only, an unknown silica layered phase similar to that observed by Cambor et al. [36] was

obtained (Fig. 1d). When vanadium was added in the synthesis containing only TMAdaOH, an amorphous solid was obtained (Fig. 1b). This result shows that the cooperative effect between TMAdaOH and HMI is critical to crystallize the MWW phase, both as all-silica [36] and also from vanadium-containing gels. An in-depth discussion of all-silica MWW phase concerning the TMAdaOH and HMI mixture was reported by Cambor et al. [36]. Based on this prior knowledge, we suggest that the filling of the sinusoidal pores by HMI seems to be required for the formation of the MWW phase containing vanadium too. In this cooperative phenomenon, the HMI molecules stabilize part of the structure in which TMAdaOH has no access due to steric impediments generated by the structure (typically, the sinusoidal 10 MR pores). The TMAdaOH is preferably located between the sheets, while the HMI molecule fills the channels within the sheets.

3.2. Effect of vanadium source and synthesis atmosphere

VOSO₄ was also used as vanadium source to verify the influence of the initial oxidation state of the vanadium precursor. Additionally, the effect of synthesis atmosphere was also investigated to evaluate the need to prevent the oxidation of VCl₃. These studies were carried out for samples prepared with a Si/V nominal ratio of 30 (Fig. 2).

In the absence of TMAdaOH (MCM-22 method) and using VOSO₄ as a vanadium source, an amorphous solid was obtained. This shows that regardless the vanadium source, the MCM-22 synthesis performed using only HMI was not effective to promote the crystallization of the MWW-type zeolite. On the contrary, the ITQ-1 synthesis performed by using

both templates simultaneously led to solid with the characteristic diffraction pattern of the MWW structure, with both VCl₃ and VOSO₄, under air or nitrogen. However, both samples synthesized under air present a white color, very similar to the sample obtained without vanadium. This observation could indicate a low incorporation of vanadium in the structure when the synthesis was performed under air, either using VCl₃ or VOSO₄. Actually, the chemical analysis (Table 1) showed that the amount of vanadium incorporated into the crystals when the synthesis was performed under air is much lower than in the samples synthesized under N₂ atmosphere. The vanadium amount incorporated in the crystals was about 3 and 7 times lower for VOSO₄ (9V-ITQ-1) and VCl₃ (10V-ITQ-1), respectively, than those found in the sample synthesized under N₂ atmosphere (samples 3V and 4V). The vanadosilicate samples obtained under N₂ atmosphere with Si/V = 30 are green before drying and light gray after drying. This is an additional indicative that the vanadium was efficiently incorporated. Therefore, the combination of VCl₃ and the preparation of the gel under inert atmosphere (N₂) are required for the successful and efficient crystallization of V-ITQ-1 with high vanadium content.

The DR-UV-Vis results shown in Fig. 2 illustrate the structural changes obtained using different preparation protocols. All spectra were collected under air before calcination (as-synthesized samples). The spectra for all samples exhibited absorption bands centered at 270 and 345 nm, which are attributed to $\pi(t_2) \rightarrow d(e)$ and $\pi(t_1) \rightarrow d(e)$ oxygen-to-tetrahedral V charge transfer transitions (CT). Several publications in literature showed [7,45–48] two types of tetrahedral sites on MEL, BEA and MFI frameworks: a more distorted site and a less distorted site with bands located at 270 and 345 nm, respectively. The sample synthesized using VCl₃ under N₂ atmosphere exhibits a distinctly high absorption level compared to the other samples. This agrees with the chemical analysis (Table 1), showing that the atmosphere used for the synthesis and the vanadium precursor have an important influence on the amount of heteroatom incorporation. Besides, the EDS analysis provided a very useful information about the chemical homogeneity. While for ITQ-1 - VCl₃ - N₂ sample, vanadium was found homogeneously distributed, for the other samples vanadium could not be detected in some regions (Fig. S1, Supplementary Data), which strongly suggests that they are most probably composed of a mixture of all-silica ITQ-1 and the vanadosilicate.

3.3. Effect of Si/V ratio

The effect of the Si/V ratio of the synthesis gel on the crystallization of the MWW phase using a combination of both OSDA (ITQ-1 route), and VCl₃ as vanadium source under N₂ atmosphere has been investigated. The XRD profiles of the as-synthesized samples with different Si/V ratio (Fig. 3) are consistent with the formation of well-ordered and pure MWW structure. Note that as the amount of vanadium increases in the synthesis mixture the intensity of the diffraction lines decrease. However, no evidence of the presence of amorphous material was found by SEM for Si/V = 30 or higher (Fig. 4). No significant differences between the synthesis times of 7 and 14 days were observed, and for 7 days the structure appears already well crystallized.

The SEM images (Fig. 4) for all-silica sample and those with Si/V ratio of 60 and 30 revealed a very similar morphology of spherical particles formed of MWW crystals. The size of particles is very heterogeneous, the images show larger particles of 20–40 μm , others of 10 μm and smaller particles showing sizes between 1 and 3 μm . The image with higher magnification shows the smaller particles in the sample synthesized with Si/V ratio of 30. The morphology is very similar to the well-known desert rose, which is made up by clusters of thin plates. Observing in more detail the images of the sample with the highest V content (Si/V ratio of 20) (Fig. 4d and e), it can be noticed that the large amount of vanadium begins to affect crystallization. The morphology observed is a mixture of heterogeneous material, perhaps amorphous phases, with MWW platelet crystals. The HRTEM images

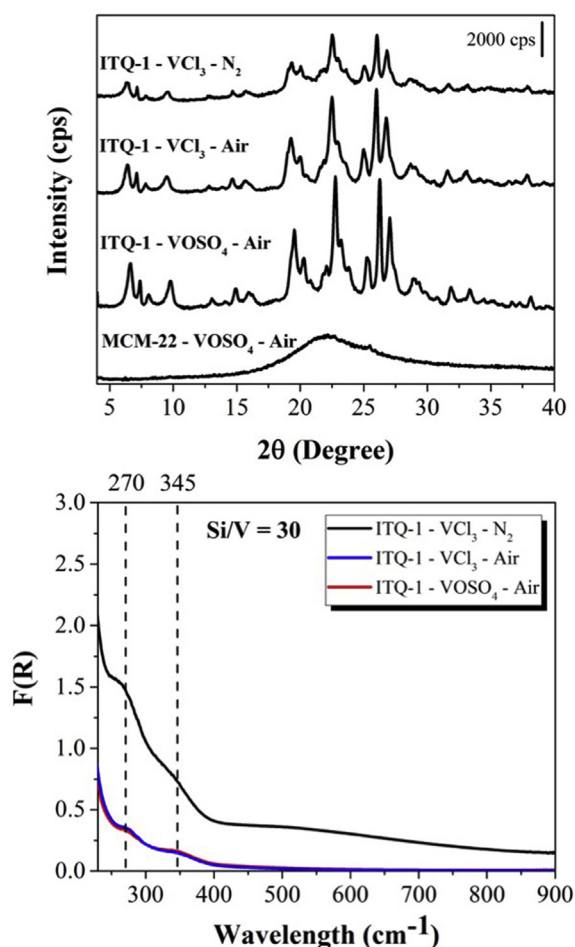


Fig. 2. XRD results (above) and DR-UV-Vis (below) for samples synthesized using different vanadium source under air or N₂ atmosphere. Synthesis conditions: Si/V = 30, 150 °C for 7 days under stirring.

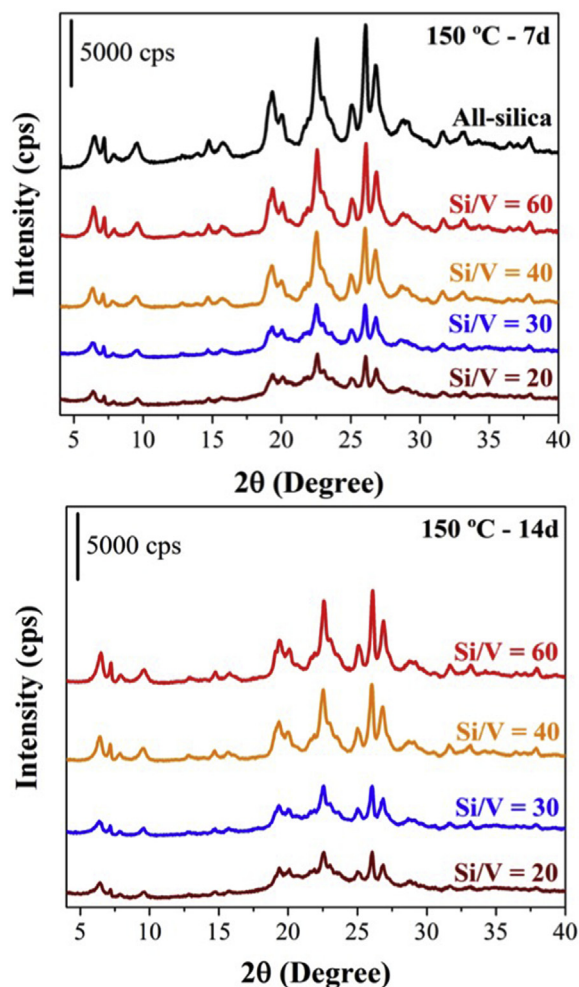


Fig. 3. XRD patterns of samples obtained after 7 (above) and 14 days (below) of ITQ-1 synthesis with different Si/V ratio in the synthesis gel.

(Fig. S2, Supplementary Data) of as-synthesized samples precursor (Si/V = 30 and 60) revealed the layered structure of the platelets observed in Fig. 4b and c. The thickness of the MWW sheets in the range of 40–50 nm, results from the stacking of the MWW layers in the [002]. The presence of this well crystallized layered structure shows that the

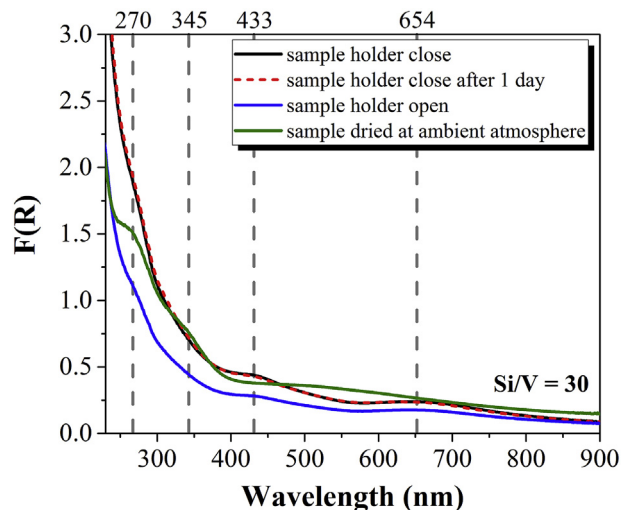


Fig. 5. The DR-UV-Vis spectra of the ITQ-1 sample synthesized with Si/V ratio 30 after 7 days of synthesis.

vanadium insertion does not affect the formation of the MWW framework.

The ITQ-1 sample with Si/V ratio of 30 was dried under N_2 atmosphere and transferred to the UV-Vis sample holder inside of a glove bag. It has been characterized in detail using DR-UV-Vis, and the results are shown in Fig. 5. Until this measurement condition, the sample showed green coloration similar to the initial gel. After that, the sample holder was opened, exposed to air, and submitted again for characterization. The black curve is superimposed on the dotted red curve, showing that no changes are observed when the sample holder was kept closed, at least for one day. When air exposure was avoided, two additional absorption bands between 400–500 nm and 600–700 nm that are characteristic of vanadium with low oxidation state (V^{3+}) [49–51] are observed. These two bands are related to isolated V^{3+} in tetrahedral coordination isomorphically substituted in the zeolite framework. This result clearly evidences that low oxidation state vanadium species are initially incorporated. After exposure of the sample to ambient atmosphere, the bands at 433 and 654 nm decreased in intensity indicating the partial oxidation of the vanadium sites. A progressive change from green to gray color was observed after exposure of the sample to the ambient atmosphere and bands in the region of 270 and 344 nm become more evident for the sample dried at ambient temperature. These

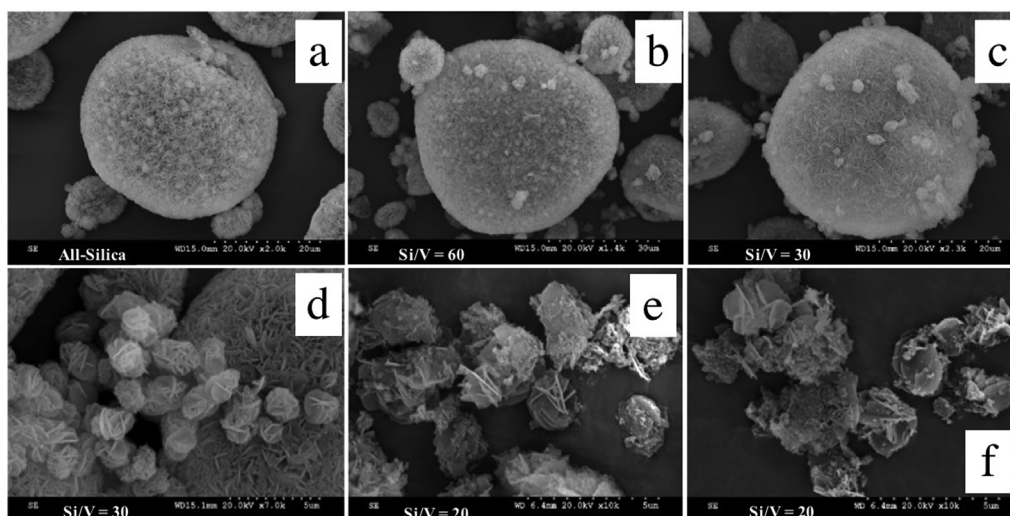


Fig. 4. SEM images for samples all-silica (a) and those with Si/V = 60 (b), 30 (c and d) and 20 (e and f).

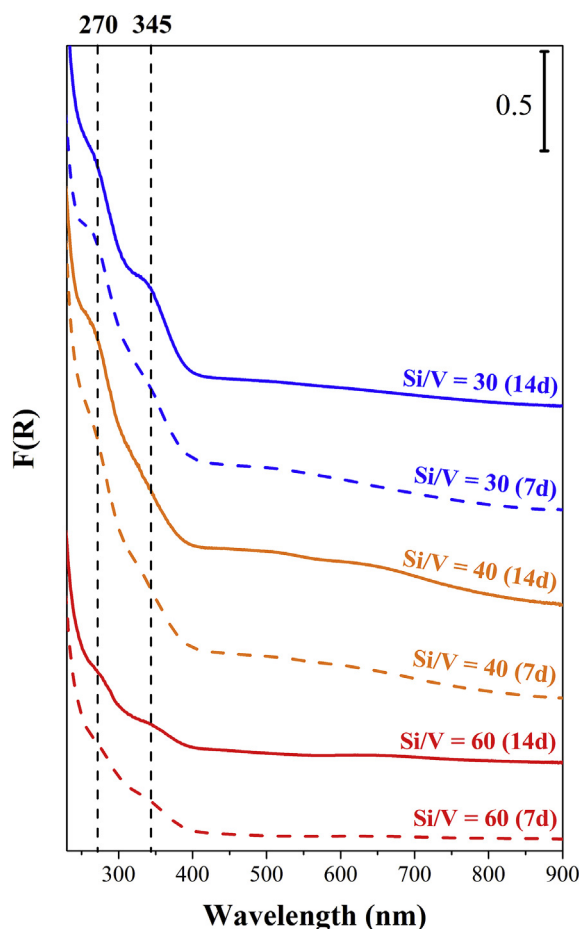


Fig. 6. DR-UV-Vis spectra of samples with different Si/V ratio obtained after 7 or 14 days of ITQ-1 synthesis.

two absorption bands, at 270 and 345 nm, are characteristic of tetrahedrally coordinated V species in the framework [7,52] and this is further evidence of the oxidation process from V^{3+} to V^{4+} .

The coordination environment of samples obtained with Si/V ratio 30, 40 and 60 were investigated by DR-UV-Vis spectroscopy (Fig. 6). The spectra of all samples present also two main absorption bands at 270 and 345 nm, which are characteristic of tetrahedrally coordinated V species in the framework. The intensity for all absorption bands increases with the vanadium amount. In addition, absorption bands of small intensity at 450 and 650 nm attributed to V^{3+} are detected, indicating that not all the V^{3+} initially present in the samples has been oxidized to V^{4+} species [50,51] upon exposure to air. The as-synthesized samples did not exhibit any band in the region around 400 nm, suggesting the absence of detectable amounts of vanadium in octahedral environments [48] and showing that V–O–V bonds are not present.

^{13}C CP-MAS NMR results are shown in Fig. 7 for all-silica samples and those obtained with Si/V = 30 and 60. The spectra show that both OSDA are present in the as-synthesized material, and no evidences of eventual decomposition products are found. The signals at 50.2, 30.7 and 27.4 ppm are associated to the chemical shifts of carbon 1, 2 and 3 in HMI, respectively, while those at 35.4, 36.1, 72.5 and 47.6 are related to carbon 5, 6, 7 and 8 in TMAdaOH, respectively. The samples synthesized with vanadium present a spectrum similar to the all-silica sample, only a variation in the intensities of the resonances 1 and 8 was observed. These results show again that the mixture of templates (TMAdaOH and HMI) is crucial for obtaining the MWW phase both without and with vanadium [36,53].

The TGA and DTG curves of the as-synthesized all-silica sample and

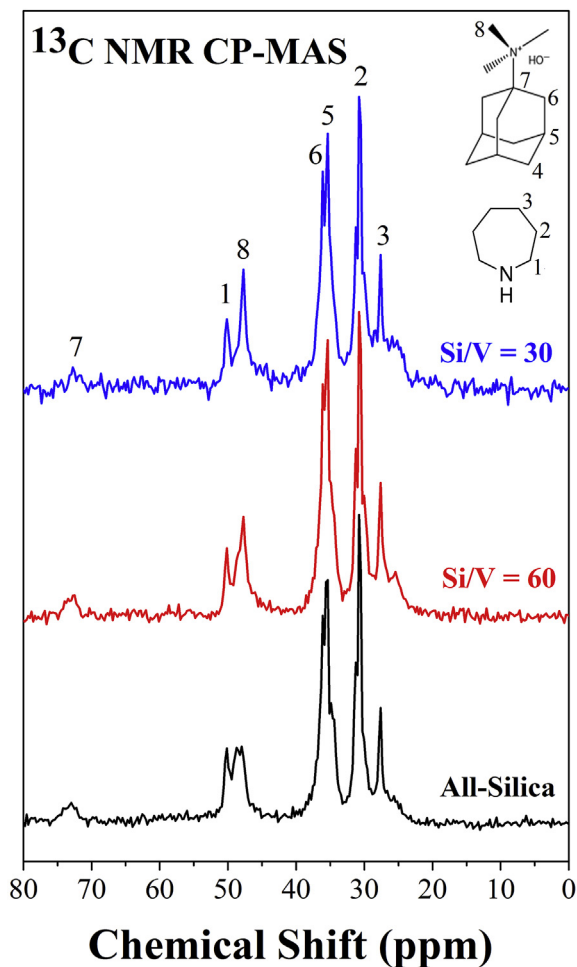


Fig. 7. ^{13}C CP-MAS NMR spectra for as-synthesized all-silica samples, Si/V = 60 and 30.

of those with Si/V ratio of 30 and 60 are shown in Fig. 8. All the samples present three main events, with a first weight loss below 100 °C associated to adsorbed water molecules and successive events above 200 °C ascribed to OSDA decomposition with different interactions with the inorganic framework located in the interlayer space. It is observed that the amount of OSDA decreases with the addition of vanadium. The total weight loss above 200 °C decreased from 22% in the all-silica sample to ~14% in the sample with Si/V ratio of 30 sample (Table 1). The mass loss in the 200–350 °C temperature range is probably due to the removal of HMI and/or TMAdaOH located on the external surface or interacting weakly with the structure. The weight loss around 400 °C is related to removal of OSDA located on interlayer arrangement whereas the last event occurs at around 600 °C and it is probably related to OSDA filling the microporous channel having a strong interaction with the framework [35,54,55]. In fact, the CNH analysis (Table 1) shows that the C/N ratio is equal to ~10.2, which suggests that the incorporation of TMAdaOH and HMI on MWW occurs in equal amounts (typically C/N = 9.7). This result is quite similar to that reported by Cambor et al. [36]. The addition of vanadium does not modify significantly the proportion between the two templates and the C/N ratio values remain around 10.2. The results obtained by CHN analysis show that insofar as vanadium is incorporated, the total amount of organic compounds decreases; similar tendency was also observed in TG results. On the other hand, the weight loss at $T > 200$ °C is higher than the amount of organic material determined by chemical analysis, due to the desorption of water coming from the condensation of Si–OH groups. It will be shown below that the observed decrease in the amount of

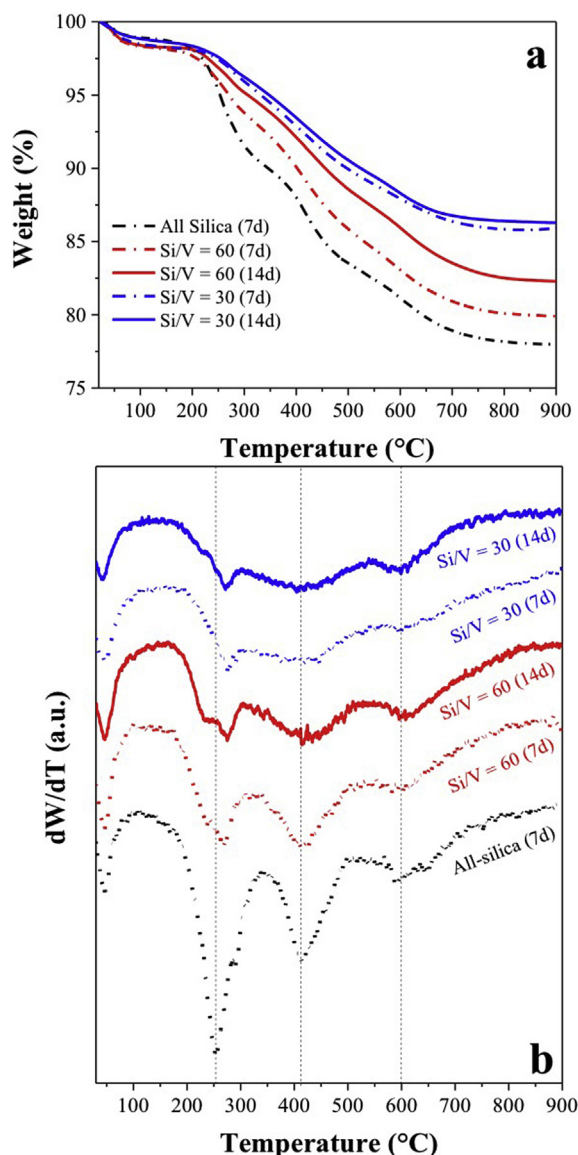


Fig. 8. TG (a) and DTG (b) analysis for sample synthesized without vanadium and with Si/V ratio 60 and 30.

organic material as the V content increases could be due to the mechanism of V incorporation in the crystals.

Adsorption/desorption isotherms of the calcined all-silica materials and those with Si/V ratios 60 and 30 shown in Fig. S3 (Supplementary Data) yielded type-I curves, characteristic of microporous structures. The adsorption profile of the sample with Si/V ratio of 30 exhibited a gradual increase of nitrogen adsorption with pressure that is typical of adsorption on the external surface of sheets. The external specific area (Table S1) for MWW samples were 48, 140 and 28 m²/g for all-silica, Si/V = 30 and 60, respectively. The important improvement of the external surface area of the sample with Si/V of 30 are within a range of values reported for the MWW structure [53].

The effect of vanadium incorporation on the chemical environment of the silicon species was analyzed from the ²⁹Si MAS NMR spectra of selected samples, shown in Fig. 9. Four resonance signals can be distinguished at -119, -116, -114 and -110 ppm, which have been also observed in all-silica ITQ-1 materials and assigned to Q⁴ sites, corresponding to Si atoms in different crystallographic sites [36]. The intense band observed at ca. -94 ppm has been attributed to Q³ configurations corresponding to Si(3Si,1OH) or Si(3Si,O⁻) siloxy defect

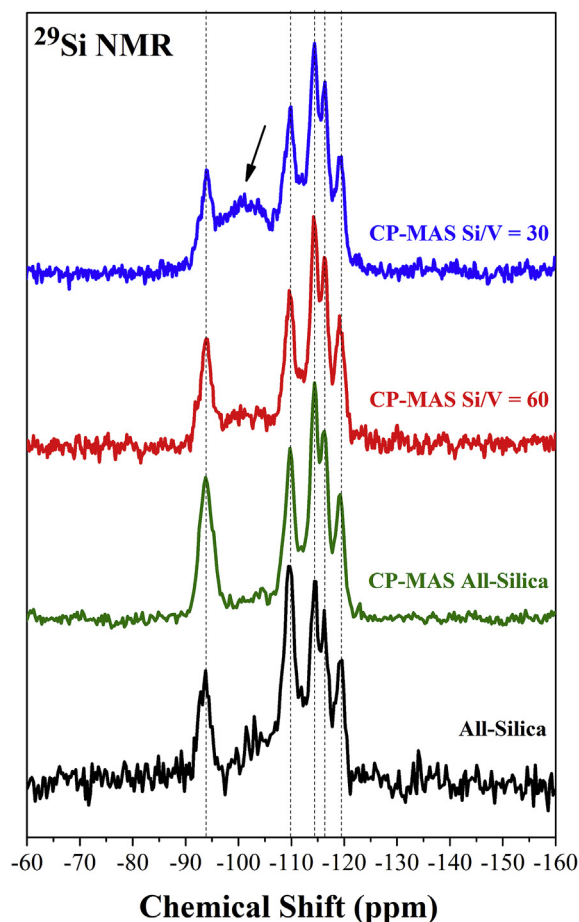


Fig. 9. ²⁹Si NMR MAS and CP-MAS spectra for as-synthesized samples all-silica, Si/V = 60 and 30.

[36,56]. Comparing the spectra with (Fig. 9, black curve) and without cross-polarization (CP) of the all-silica samples, we can observe that the chemical shift at ca. -94 ppm is more intense when the cross polarization analysis is performed. This result indicates that a neighbor near the silicon atom is a proton. The chemical shift at -103 ppm is suppressed indicating the presence of siloxy groups. For the vanadosilicates, a new band around -103 ppm is detected, (indicated by an arrow) whose intensity increases with the V content, that can be attributed to Q⁴ environments where one Si atom would be bonded to V in Si-O-V configuration (Si(3Si,1V) [57,58]. Beside this, the signal at ca. -94 ppm decreases in intensity, showing that the amount of defects of Q³ type decreases with the vanadium incorporation in the structure and that, probably, the vanadium incorporation occurs preferentially in this kind of site. This is an additional evidence that the vanadium is incorporated efficiently into the zeolite framework. Thus, with the isomorphous substitution of vanadium, a smaller amount of Q³ sites was observed and, consequently, a smaller amount of OSDA is required to compensate the defects in the structure, in agreement with TG results.

3.4. Vanadium local order for ITQ-1 with Si/V = 30

The in-depth NMR characterization of samples prepared according to the ITQ-1 method converges towards the incorporation of vanadium inside the zeolitic network. In order to confirm this assumption, the ITQ-1 sample prepared from VCl₃ and under inert atmosphere at Si/V ratio = 30 has been characterized at 77K by X-ray absorption spectroscopy. The sample was not preserved from ambient air after preparation.

Information about the vanadium oxidation state and geometry of its

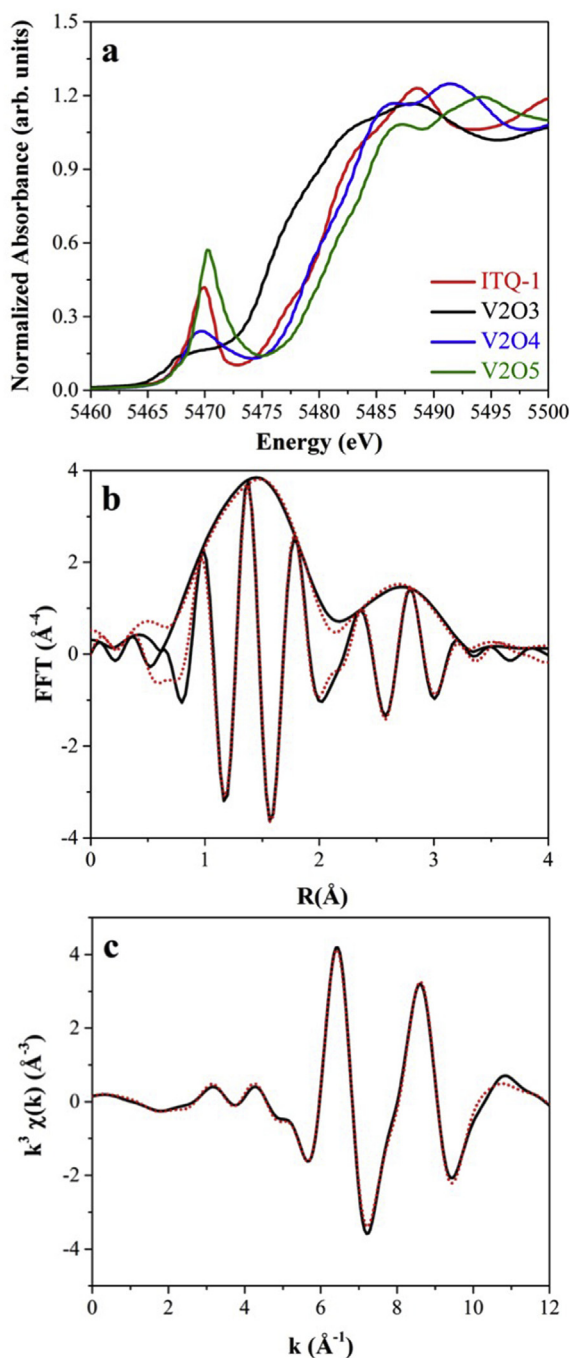


Fig. 10. V K edge XAS measurement performed on the ITQ-1 sample (Si/V = 30). (a) Zoom on the rising edge of the XANES spectrum recorded for the ITQ-1 sample and comparison with those of V_2O_3 , V_2O_4 and V_2O_5 . Extended energy-range for the spectra is shown in Fig. S2 in Supplementary Information, results of least square fittings: Comparison of (b) the magnitude and imaginary functions of Fourier Transform and (c) the real part of the EXAFS $k^3\chi(k)$ spectrum. Black lines: experimental data, red dots = fit.

first coordination sphere can be extracted from the position of the rising edge corresponding to 50% level of the normalized XANES absorbance $E_{1/2}$ and from the intensity and position of the pre-edge peak [59–61]. Fig. 10a compares the XANES spectrum of the ITQ-1 sample (Si/V = 30) with those of oxide references at different oxidation states, V_2O_3 , V_2O_4 , V_2O_5 . The position of the rising edge for the sample ($E_{1/2} = 5479.4$ eV) is consistent with the formation of tetravalent vanadium species ($E_{1/2} = 5479.2$ eV for V_2O_4), as observed by UV–Vis spectroscopy for samples not preserved from oxidation after synthesis. It is also

Table 2

Refined structural parameters for the sample ITQ1 (Si/V = 30) from least square fitting of the EXAFS spectra recorded at the V K edge. S_0^2 was determined to be 1.16 on V_2O_4 and was kept at this value for the fitting of samples, ΔE_0 was also fixed at 5479.1 eV. Fit were performed on R-space for Fourier Transforms of the $k^3\chi(k)$ EXAFS spectra carried out in the 4.0–10.0 \AA^{-1} k-range. The coordination numbers for the 2nd nearest neighbours were fixed.

Backscatterer	N	R (\AA)	σ^2 (\AA^2) $\times 10^3$	R-factor
O	1.5 ± 0.3	1.64 ± 0.01	5.2 ± 1.7	
O	3.8 ± 0.8	1.99 ± 0.01	14.3 ± 2.5	
O	2.0 ± 0.4	3.03 ± 0.02	7.6 ± 2.6	0.0050
Si	1.0 ± 0.2	3.26 ± 0.02	7.7 ± 3.1	

noted that the pre-edge intensity is higher for the ITQ-1 sample than the one of V_2O_4 , suggesting a less centrosymmetrical coordination for vanadium than the octahedral one characterizing V_2O_4 [59].

Structural parameters obtained for fitting in R-space the Fourier Transform of the ITQ-1 sample (Si/V = 30) are gathered in Table 2, whereas the results of the $k^3\chi(k)$ EXAFS fitting in R space is presented in Fig. 10b and c, in R-space and k-space, respectively. In agreement with the intensity of the pre-edge structure, the first coordination shell of ITQ-1 sample could be described as a square-pyramidal geometry with a short V=O distance at 1.64 \AA and equatorial longer V–O bonds at 1.99 \AA . The second contribution in the Fourier Transform is satisfactorily described by additional V–O contribution at 3.03 \AA and V–Si contribution at 3.26 \AA . It is noteworthy that for keeping the number of fitted parameters at a value satisfying the Nyquist criterion [44] (herein $N_{\text{ind}} = 10 = N_{\text{fitted par.}}$), the coordination numbers for those contributions were fixed at 2 and 1, respectively. Several coordination number values for those contributions were used for the simulations and those reported in Table 2 are the best ones regarding the statistical parameters related to each fit. The medium range order around Vanadium in the ITQ-1 sample are in agreement with the distances reported for the ITQ-1 sample are in agreement with distances found in the cavansite ($\text{Ca}(\text{VO})\text{Si}_4\text{O}_{10}\cdot 4\text{H}_2\text{O}$) [62] structure containing square pyramidal V^{4+} environment with a short V–O bond at 1.60 \AA and 4 equatorial V–O bonds at 1.975 \AA and contributions of 2 Si at 3.22 \AA , and 2 Si atoms at 3.33 \AA . The longer V–O contribution at 3.03 \AA is ascribed to water molecules, as it can be also found in cavansite structure. XAS results are then fully consistent with the afore discussed NMR results and allows us to conclude that the ITQ-1 synthesis protocol leads to the incorporation of isolated vanadium in the lattice of the MWW structure with formation of linkage between V and Si atoms through O bridges.

3.5. Thermal stability of the ITQ-1

The thermal stability of the sample with Si/V ratio of 30 was evaluated by monitoring *in situ* the calcination process under air by X-ray diffraction (Fig. 11). The precursor MWW presents several peaks in the 4–12° 2θ range related to planes (002), (100), (101) and (102). The plane (002) is characteristic of the distance between the sheets of the MWW structure [29,63]. After 200 °C the peak (002) begins to move to larger angles showing that at this temperature the lamellar precursor starts the process of condensation of the MWW sheets. TG results also show mass loss in this temperature range related to the removal of interlamellar organic material. Above 300 °C there is a decrease in the intensity of the (002) reflection that is no longer observed at 450 °C. Its disappearance is related to the condensation of the MWW sheets and the formation of the three-dimensional MWW structure. Up to 500 °C the MWW crystalline phase is maintained without changes in the intensities of the diffraction peaks.

The stability of the calcined ITQ-1 samples with Si/V ratio of 30 and

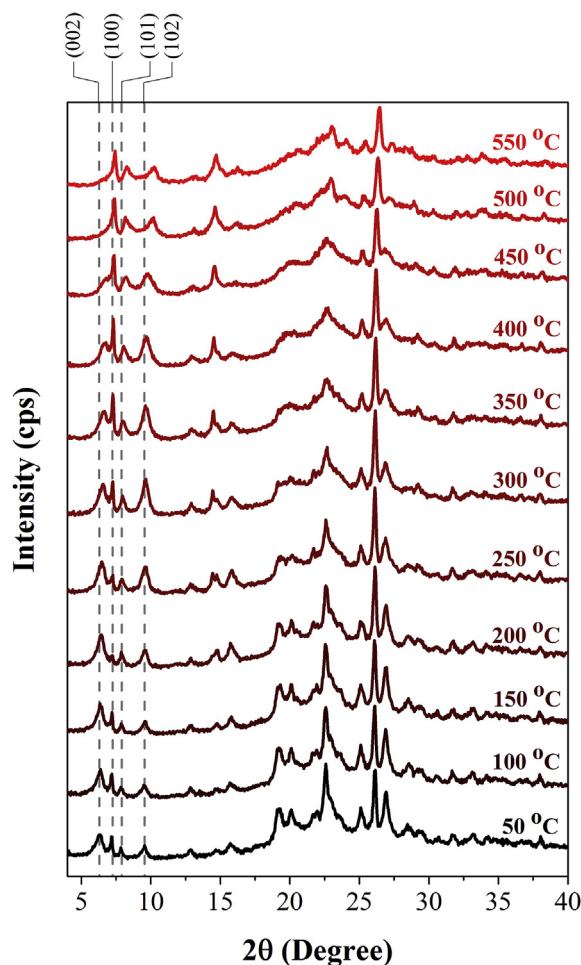


Fig. 11. X-Ray diffraction patterns evolution during calcination under air atmosphere for the sample obtained with $\text{Si}/\text{V} = 30$.

60 ratio was confirmed by the DR-UV-Vis spectra (Fig. S4, Supplementary Data), showing the two main bands centered at 270 and 378 nm characteristic of the isolated VO_4 in tetrahedral sites and to V^{5+} in octahedral coordination, respectively. Additionally, for the sample Si/V ratio of 60 a shoulder was observed at around 230 nm, which may be related to more distorted tetrahedral sites [64]. Moreover, the absence of a band at 500 nm in the DR-UV-Vis spectra is an indicative of the absence of V_2O_5 crystallites after calcination [65].

Fig. 12 displays the time-resolved V K edge Quick-XANES spectra evolution versus temperature during calcination of the sample ITQ-1 ($\text{Si}/\text{V} = 30$) under air atmosphere. The Quick-XAS *in situ* measurement showed that the pre-edge peak intensity increases continuously upon heating and the shape of the different XANES features changes gradually. The phase speciation of vanadium during calcination was determined by MCR-ALS analysis. The oxidation of the initial V^{4+} species starts at 245 °C and is completely oxidized to V^{5+} after 20 min at 550 °C. At the end of the plateau at 550 °C (Fig. S5, Supplementary Data), the $E_{1/2}$ position is 5481 eV and the pre-edge maximum at 5470.1 eV. These values are consistent with V^{5+} species in Td-symmetry [66] similar to the one encountered in aqueous solution of $(\text{NH}_4)\text{VO}_3$, as displayed in Fig. S6. The simulation of the EXAFS signal of this V^{5+} species after cooling down at RT agrees also with this 4-fold tetrahedral coordination with 1.5 O at $1.61 \pm 0.03 \text{ \AA}$ and $2.5 \pm 0.4 \text{ O}$ at $1.81 \pm 0.04 \text{ \AA}$ (Table S2, Supplementary Data). As for the $(\text{NH}_4)\text{VO}_3$ aqueous solution, the Fourier transformed EXAFS spectra of the V^{5+} calcined species does not present medium range order beyond the first coordination shell (Fig. S7, Supplementary Data). This finding is indicative of the presence of completely isolated vanadium sites [59,67]

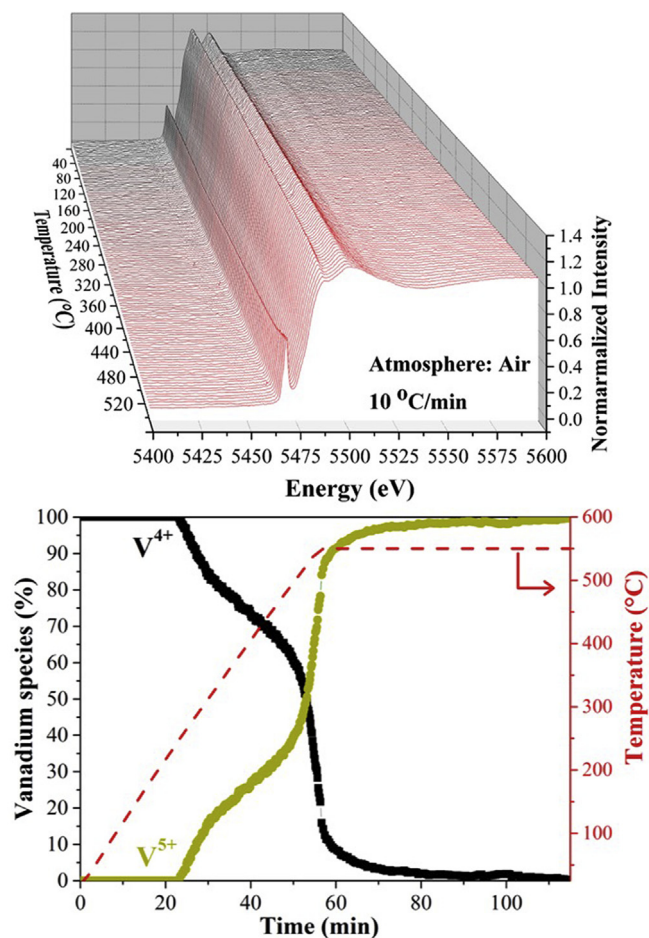


Fig. 12. Evolution of the V K edge XANES Quick-XAS spectra collected during calcination: (above) RT to 550 °C and (below) concentration profiles of vanadium species involved during calcination by MCR-ALS analysis.

after calcination. The results obtained by XAS corroborate the DR-UV-Vis results discussed previously, confirming the V local structural features expected for the isomorphous substitution of vanadium in the zeolite framework.

Finally, a side contribution of this in depth characterization of the local structure of vanadium and silicon atoms in ITQ-1 samples concern the origin of the vibrational (IR and Raman) band around 960 cm^{-1} . Generally, this band was used as a characteristic fingerprint of isomorphous substitution of silicon in zeolite framework, but it can be also due to silanol groups or siloxy defect sites ($\text{Si}-\text{O}$) [68–71]. It is shown in Figs. S8a and S8b an experimental infrared spectra acquired in ATR mode where the band at 965 cm^{-1} is present in both as-synthesized and calcined all-silica and vanadosilicate MWW samples. These results demonstrate that this band is also related to silanol and/or siloxy defect.

4. Conclusions

This paper reports the preparation route of new vanadosilicates with MWW structure and highlights the important parameters for achieving the effective incorporation of vanadium into the zeolite framework. V-MWW was synthesized by using a cooperative assembly between the organic templates TMAOH and HMI in the presence of VCl_3 . According to ^{13}C CP-MAS NMR, both templates are present in the as-synthesized sample. Besides, low oxidation state vanadium source (VCl_3) and the preparation under inert atmosphere are necessary to ensure vanadium incorporation. In the as-made unoxidized sample, isolated vanadium with low oxidation state (V^{3+}) is present in

tetrahedral coordination. When exposed to ambient atmosphere, V^{3+} species are mainly oxidized to V^{4+} . The ^{29}Si MAS NMR results indicate high structural similarity between all-silica ITQ-1 and the vanadosilicate samples. The dependence of the intensity of the resonance around -103 ppm attributed to $(\text{Si}(3\text{Si},1\text{V}))$ environments with the vanadium loading was a first indirect evidence of the isomorphic substitution of silicon by vanadium atoms into the MWW framework. Such incorporation is fully confirmed by EXAFS analysis, showing that the second coordination shell of vanadium atoms of an ITQ-1 sample (with $\text{Si}/\text{V} = 30$) is properly reproduced using a $\text{V}-\text{Si}$ contribution at 3.26 \AA , evidencing the presence of isolated V sites and the presence of $\text{V}-\text{O}-\text{Si}$ linkages. Moreover, XAS results showed that as-synthesized V-MWW samples exposed to ambient atmosphere are made of isolated V^{4+} square pyramidal sites. Upon calcination under air up to $550 \text{ }^\circ\text{C}$, X-ray diffraction measurements highlights the thermal stability of the MWW framework, whereas time-resolved XAS measurements evidences the oxidation of the network former V^{4+} species into isolated V^{5+} ones in Td symmetry. Vanadium-containing catalysts are widely used in several oxidation reactions, and we believe that the Al-free MWW vanadosilicates obtained by the first time in this work may have potential to be applied on this kind of reactions.

Acknowledgments

The authors acknowledge financial support by grant 2014/11952-5 and 2015/25850-2 by São Paulo Research Foundation (FAPESP). XAS measurements were supported by a public grant overseen by the French National Research Agency (ANR) as part of the “Investissements d’Avenir” program (reference: ANR-10- EQPX-45). The authors are grateful to SOLEIL committees for beam time available on ROCK beamline (Proposal ID 20160946). We also thank to Prof. Miguel A. Cambor for the discussion about the ITQ-1 synthesis and to Perrine Chaurand (Cerege, France) for the fruitful discussion on the cavansite structure. Thanks to SACHEM company for the kind donation of TMAdaOH used in this work.

Appendix A. Supplementary data

Supplementary data to this article can be found online at <https://doi.org/10.1016/j.micromeso.2018.12.030>.

References

- [1] C.S. Cundy, P.A. Cox, *Chem. Rev.* 103 (2003) 663–701.
- [2] C.S. Cundy, P.A. Cox, *Microporous Mesoporous Mater.* 82 (2005) 1–78.
- [3] M. Taramasso, G. Perego, B. Notari, Preparation of Porous Crystalline Synthetic Material Comprised of Silicon and Titanium Oxides, (1983) US Patent 4, 410, 501.
- [4] G. Bellussi, M.S. Rigutto, *Stud. Surf. Sci. Catal.* 85 (1994) 177–213.
- [5] A. Corma, *J. Catal.* 216 (2003) 298–312.
- [6] G. Genti, S. Perathoner, F. Trifiro, a. Aboukai, C.F. Aissi, M. Guelton, *J. Phys. Chem.* 96 (1992) 2617–2629.
- [7] T. Sen, V. Ramaswamy, S. Ganapathy, P.R. Rajamohanam, S. Sivasanker, *J. Phys. Chem.* 100 (1996) 3809–3817.
- [8] X. Tang, L. Pan, J. Wang, H. Li, *Stud. Surf. Sci. Catal.* 154 (2004) 1356–1362.
- [9] A. Tuel, Y.B. Taarit, *Appl. Catal. A Gen.* 102 (1993) 201–214.
- [10] A. Albuquerque, L. Marchese, L. Lisi, H.O. Pastore, *J. Catal.* 241 (2006) 367–377.
- [11] F. Mani, J.A. Sawada, S.M. Kuznicki, *Microporous Mesoporous Mater.* 224 (2016) 208–216.
- [12] D. Wei, H. Wang, X. Feng, W. Chueh, P. Ravikovitch, M. Lyubovskiy, C. Li, T. Takeguchi, G.L. Haller, *J. Phys. Chem. B* (1999) 2113–2121.
- [13] M. Morey, A. Davidson, H. Eckert, G. Stucky, *Chem. Mater.* 8 (1996) 486–492.
- [14] L.H. Vieira, L.G. Possato, T.F. Chaves, S.H. Pulcinelli, C.V. Santilli, L. Martins, *Mol. Catal.* 458 (2018) 161–170.
- [15] T.H. Abreu, C.I. Meyer, C. Padró, L. Martins, *Microporous Mesoporous Mater.* 273 (2019) 219–225.
- [16] K.M. Jinka, H.C. Bajaj, R.V. Jasra, E.A. Prasetyanto, S.-E. Park, *Top. Catal.* 53 (2010) 238–246.
- [17] N.K. Mal, A.V. Ramaswamy, *Appl. Catal. A Gen.* 143 (1996) 75–85.
- [18] A.V. Ramaswamy, S. Sivasanker, P. Ratnasamy, *Microporous Mater.* 2 (1994) 451–458.
- [19] P.R. Hari Prasad Rao, A.V. Ramaswamy, P. Ratnasamy, *J. Catal.* 137 (1992) 225–231.
- [20] T. Zhang, L. Mazaud, L.-M. Chamoreau, C. Paris, A. Proust, G. Guillemot, *ACS Catal.* 8 (2018) 2330–2342.
- [21] M.G. Clerici, *Kinet. Catal.* 56 (2015) 450–455.
- [22] A. Chieregato, M.D. Soriano, F. Basile, G. Liosi, S. Zamora, P. Concepción, F. Cavani, J.M. López Nieto, *Appl. Catal. B Environ.* 150–151 (2014) 37–46.
- [23] L.G. Possato, W.H. Cassinelli, T. Garetto, S.H. Pulcinelli, C.V. Santilli, L. Martins, *Appl. Catal. A Gen.* 492 (2015) 243–251.
- [24] K.-W. Park, J. Hwa, H.-J. Seo, O.-Y. Kwon, *Microporous Mesoporous Mater.* 121 (2009) 219–225.
- [25] T. Lv, S. Zhang, Z. Feng, F. Wang, S. Zhang, J. Zheng, X. Liu, C. Meng, Y. Wang, *Cryst. Growth Des.* 17 (2017) 3940–3947.
- [26] S. Inagaki, Y. Sakamoto, Y. Fukushima, O. Terasaki, *Chem. Mater.* 8 (1996) 2089–2095.
- [27] F.S.O. Ramos, M.K. de Pietre, H.O. Pastore, *RSC Adv.* 3 (2013) 2084–2111.
- [28] N. Takahashi, K. Kuroda, *J. Mater. Chem.* 21 (2011) 14336–14353.
- [29] A. Corma, V. Fornes, S.B. Pergher, T.L.M. Maesen, J.G. Buglass, *Nature* 396 (1998) 353–356.
- [30] M.E. Leonowicz, J.A. Lawton, S.L. Lawton, M.K. Rubin, *Science* 80 (264) (1994) 1910–1913.
- [31] A. Alfayate, C. Márquez-Álvarez, M. Grande-Casas, B. Bernardo-Maestro, M. Sánchez-Sánchez, J. Pérez-Pariente, *Catal. Today* 213 (2013) 211–218.
- [32] A. Alfayate, M. Sánchez-Sánchez, J. Pérez-Pariente, *Microporous Mesoporous Mater.* 190 (2014) 334–345.
- [33] A. Alfayate, C. Márquez-Álvarez, *Catal. Today* 227 (2014) 57–64.
- [34] A. Alfayate, R. Sepúlveda, M. Sánchez-Sánchez, J. Pérez-Pariente, *Top. Catal.* 59 (2016) 326–336.
- [35] A. Corma, C. Corell, J. Pérez-Pariente, *Zeolites* 15 (1995) 2–8.
- [36] M.A. Cambor, A. Corma, M.-J. Diaz-Cabañas, C. Baerlocher, *J. Phys. Chem. B* 102 (1998) 44–51.
- [37] S. Storck, H. Bretinger, W.F. Maier, *Appl. Catal. A Gen.* 174 (1998) 137–146.
- [38] V. Briois, C. La Fontaine, S. Belin, L. Barthe, T. Moreno, V. Pinty, A. Carcy, R. Girardot, E. Fonda, *J. Phys. Conf. Ser.* 712 (2016) 12149.
- [39] C. La Fontaine, L. Barthe, A. Rochet, V. Briois, *Catal. Today* 205 (2013) 148–158.
- [40] A. Rochet, B. Baubet, V. Moizan, C. Pichon, V. Briois, *Compt. Rendus Chem.* 19 (2016) 1337–1351.
- [41] W.H. Cassinelli, L. Martins, A.R. Passos, S.H. Pulcinelli, C.V. Santilli, A. Rochet, V. Briois, *Catal. Today* 229 (2014) 114–122.
- [42] B. Ravel, M. Newville, *J. Synchrotron Radiat.* 12 (2005) 537–541.
- [43] J.M. Longo, P.A. Kierkegaard, *Acta Chem. Scand.* 24 (1970) 420–426.
- [44] E.A. Stern, *Phys. Rev. B* 48 (1993) 9825–9827.
- [45] F. Tielens, M. Trejda, M. Ziolk, S. Dzwigaj, *Catal. Today* 139 (2008) 221–226.
- [46] P.R.H.P. Rao, R. Kumar, A.V. Ramaswamy, P. Ratnasamy, *Zeolites* 13 (1993) 663–670.
- [47] N. Venkathathri, S.G. Hegde, S. Sivasanker, *Indian J. Chem.* 42 (2003) 974–982.
- [48] M. Trejda, M. Ziolk, Y. Millot, K. Chalupka, M. Che, S. Dzwigaj, *J. Catal.* 281 (2011) 169–176.
- [49] N.H. Choi, S. -k. Kwon, H. Kim, *J. Electrochem. Soc.* 160 (2013) A973–A979.
- [50] V.S. Tripathi, K.K. Bairwa, D. Mal, D.B. Naik, *J. Electrochem. Soc.* 161 (2014) E34–E39.
- [51] M. Vijayakumar, L. Li, Z. Nie, Z. Yang, J. Hu, *Phys. Chem. Chem. Phys.* 14 (2012) 10233–10242.
- [52] S. Dzwigaj, M.J. Peltre, P. Massiani, A. Davidson, M. Che, T. Sen, S. Sivasanker, S. Mas, *Chem. Commun.* (1998) 87–88.
- [53] R. Ravishanker, D. Bhattacharya, N.E. Jacob, S. Sivasanker, *Microporous Mater.* 4 (1995) 83–93.
- [54] S.B.C. Pergher, A. Corma, V. Fornés, *Quim. Nova* 26 (2003) 795–802.
- [55] A.J. Schwanke, S. Pergher, U. Díaz, A. Corma, *Microporous Mesoporous Mater.* 254 (2017) 17–27.
- [56] M. Hunger, S. Ernst, J. Weitkamp, *Zeolites* 15 (1995) 188–192.
- [57] S. Maheshwari, E. Jordan, S. Kumar, F.S. Bates, R.L. Penn, D.F. Shantz, *M. Tsapatsis, J. Am. Chem. Soc.* 4 (2008) 1507–1516.
- [58] W. Kolodziejcki, C. Zicovich-wilson, C. Corell, J. Perez-pariente, A. Corma, *J. Phys. Chem.* 99 (1995) 7002–7008.
- [59] J. Besnardiere, X. Petrisans, F. Ribot, V. Briois, C. Surcin, M. Morcrette, V. Buissette, T. Le Mercier, S. Cassaignon, D. Portehault, *Inorg. Chem.* 55 (2016) 11502–11512.
- [60] P. Chaurand, J. Rose, V. Briois, M. Salome, O. Proux, V. Nassif, L. Olivi, J. Susini, J.-L. Hazemann, J.-Y. Bottero, *J. Phys. Chem. B* 111 (2007) 5101–5110.
- [61] J. Wong, F.W. Lytle, R.P. Messmer, D.H. Maylotte, *Phys. Rev. B* 30 (1984) 5596–5610.
- [62] J. Howard T. Evans, *Am. Mineral.* 58 (1973) 412–424.
- [63] P. Wu, T. Tatsumi, T. Komatsu, T. Yashima, *J. Phys. Chem. B* 105 (2001) 2897–2905.
- [64] G.L. Paz, E.C.O. Munsignatti, H.O. Pastore, *J. Mol. Catal. A Chem.* 422 (2016) 43–50.
- [65] P. Concepción, J.M. López Nieto, J. Pérez-Pariente, *J. Mol. Catal. A Chem.* 99 (1995) 173–182.
- [66] J. Besnardiere, X. Petrisans, F. Ribot, V. Briois, C. Surcin, M. Morcrette, V. Buissette, T. Le Mercier, S. Cassaignon, D. Portehault, *Inorg. Chem.* 38 (2016) 11502–11512.
- [67] J.A. Rees, A. Wandzilak, D. Maganas, N.I.C. Wurster, S. Hugenbruch, J.K. Kowalska, C.J. Pollock, F.A. Lima, K.D. Finkelstein, S. Debeer, *J. Biol. Inorg. Chem.* 21 (2016) 793–805.
- [68] M.R. Boccuti, K.M. Rao, A. Zecchina, G. Leofanti, G. Petrini, *Stud. Surf. Sci. Catal.* 48 (1989) 133–144.
- [69] M.A. Cambor, A. Corma, J. Perez-Pariente, *J. Chem. Soc. Chem. Commun.* 0 (1993) 557–559.
- [70] S. Bordiga, C. Lamberti, F. Bonino, A. Travert, F. Thibault-Starzyk, *Chem. Soc. Rev.* 44 (2015) 7262–7341.
- [71] A.J.M. De Man, J. Sauer, *J. Phys. Chem.* 100 (1996) 5025–5034.